ARTICLE

Photoelectron Spectroscopy and Density Functional Calculations of $TiGe_n^-$ (n=7−12) Clusters†

Xiao-jiao Deng, Xiang-yu Kong, Xi-ling Xu, Hong-guang Xu*, Wei-jun Zheng*

Beijing National Laboratory for Molecular Sciences, State Key Laboratory of Molecular Reaction Dynamics, Institute of Chemistry, Chinese Academy of Sciences, Beijing 100190, China

(Dated: Received on November 15, 2015; Accepted on December 29, 2015)

The growth pattern and electronic properties of $TiGe_n^-$ (n=7−12) clusters were investigated using anion photoelectron spectroscopy and density functional theory calculations. For both anionic and neutral $TiGe_n$ clusters, a half-encapsulated boat-shaped structure appears at n=8, and the boat-shaped structure is gradually covered by the additional Ge atoms to form Ge_n cage at n=9−11. $TiGe_{12}^-$ cluster has a distorted hexagonal prism cage structure. According to the natural population analysis, the electron transfers from the Ge_n framework to the Ti atom for $TiGe_n^{-/0}$ clusters at n=8−12, implying that the electron transfer pattern is related to the structural evolution.

Key words: Photoelectron spectroscopy, Density functional theory, Germanium clusters

I. INTRODUCTION

Experimental and theoretical studies suggested that the doping of transition metals (TMs) can stabilize the cage structures of germanium-based clusters and tailor their properties [1−5]. Ti-doped germanium clusters have attracted much attention because they may be used to produce cluster-assembled materials of special electronic and magnetic properties [6]. It has been proposed that Ti-Ge binary alloys may be developed for dental materials [7]. It has also been found that strain-released hybrid multiplayer Ge-Ti nanomembranes can form anode materials with both high conductivity and high storage capacity, therefore, enhance the performance of lithium batteries [8]. Investigating the structural and electronic properties of Ti-doped germanium clusters may provide valuable information for developing cluster-assembled materials as well as their applications in electronics, biomedicine, and energy storage. Kumar and Kawazoe conducted theoretical calculations on a number of TM-doped germanium clusters and predicted $TiGe_{16}$ cluster to be a Frank-Kasper polyhedron structure with a large gap between its highest-occupied-orbital (HOMO) and lowest-unoccupied-orbital (LUMO) [9]. In addition to the $TiGe_{16}$ cluster, the density functional theory (DFT) calculations of Bandyopadhyay *et al.* on $TiGe_n$ (n=14−20) suggested that $TiGe_{18}$ cluster also has enhanced stability [10]. The ground state structure of $TiGe_{12}$ cluster is proposed to be a remarkably stable pseudoicosahedron by Tang *et al.* [11]. More recently, the DFT calculations of $TiGe_n$ (n=1−20) clusters of Kumar *et al.* suggested that the Ti atom is encapsulated in the Ge_n cage when n is larger than 9 and the most stable structure of $TiGe_{12}$ cluster is a relaxed hexagon [12]. Compared with the theoretical studies of $TiGe_n$ clusters, the experimental investigation of $TiGe_n$ clusters is quite rare except that Nakajima and coworkers investigated $TiGe_n$ clusters using mass spectrometry and anion photoelectron spectroscopy, and probed their stability via their reactivity to H_2O adsorption [2, 13].

Previously, we have investigated the structural, electronic and magnetic properties of small size $TiGe_n^-$ (n=2−6) clusters using anion photoelectron spectroscopy and DFT calculations [14]. The results displayed that the most stable structures of these small clusters can be considered as a Ti atom substituting one of the Ge atoms in the corresponding Ge_{n+1} cluster or a Ti atom capping a Ge_n cluster, and the Ti atom is inclined to interact with more Ge atoms. In order to get more information regarding the structural evolution and electronic properties of larger $TiGe_n$ clusters, in this work, we investigated the $TiGe_n^-$ (n=7−12) clusters using mass-selected anion photoelectron spectroscopy experiments combined with DFT calculations.

II. EXPERIMENTAL AND THEORETICAL METHODS

The experiments were conducted on a home-built apparatus equipped with a laser vaporization supersonic cluster source, a time-of-flight mass spectrometer, and a magnetic-bottle photoelectron spectrometer, which has

†Part of the special issue for "the Chinese Chemical Society's 14th National Chemical Dynamics Symposium".

*Authors to whom correspondence should be addressed. E-mail: xuhong@iccas.ac.cn, zhengwj@iccas.ac.cn, Tel.: +86-10-62635054, FAX: +86-10-62563167

been described elsewhere [15]. The $TiGe_n^-$ (n=7−12) cluster anions were generated in the laser vaporization source by laser ablation of a rotating translating disk target (13 mm diameter, Ti:Ge mole ratio 1:4) with the second harmonic of a nanosecond Nd:YAG laser (Continuum Surelite II-10). The typical laser power used in this work is about 10 mJ/pulse. Helium gas with ∼4 atm backing pressure was allowed to expand through a pulsed valve (General Valve Series 9) into the source to cool the formed clusters. The generated cluster anions were mass-analyzed with the time-of-flight mass spectrometer. The cluster anions of interest were selected with a mass gate, decelerated by a momentum decelerator, and crossed with the beam of another Nd:YAG laser (Continuum Surelite II-10, 266 nm) at the photodetachment region. The electrons from photodetachment were energy-analyzed by the magnetic-bottle photoelectron spectrometer. The photoelectron spectra were calibrated with the spectra of Cu^- and Pb^- taken at similar conditions. The resolution of the magnetic-bottle photoelectron spectrometer was about 40 meV at electron kinetic energy of 1 eV.

For the $TiGe_n^{-/0}$ clusters, geometry optimizations were performed using DFT with Becke's three-parameter and Lee-Yang-Parr's gradient-corrected correlation hybrid functional (B3LYP) [16−18] and 6-311+G(d) basis sets as implemented in the Gaussian 03 program package [19]. For all clusters, a large amount of initial structures were taken into accounts at all possible spin states. These initial structures were constructed by Ti-capping or Ti-substituting of pure Ge_n clusters or based on the structures of TM-doped Ge_n clusters reported in the literature [12, 20−27]. All geometries were optimized without any symmetry constraint. Harmonic vibrational frequencies were calculated to make sure that the structures correspond to real local minima, and the zero-point vibrational energy corrections were included for the relative energies of isomers. The natural population analysis (NPA) of $TiGe_n^{-/0}$ (n=7−12) clusters were conducted with the nature bond orbital (NBO) version 3.1 program [28−34] implemented in the Gaussian 03 program package.

III. RESULTS

A. Experimental results

The photoelectron spectra of the $TiGe_n^-$ (n=7−12) clusters taken with 266 nm photons are shown in Fig.1, and the vertical detachment energies (VDEs) and adiabatic detachment energies (ADEs) of these clusters estimated from photoelectron spectra are listed in Table I. The VDEs were estimated from the maxima of the first peaks. The ADE of each cluster was determined by drawing a straight line along the leading edge of the first peak to cross the baseline of spectrum and adding the instrument resolution to electron binding energy (EBE) value at the crossing point. Our spectra are in agreement with previous measurement of $TiGe_n^-$ (n=7−17) reported by Nakijima and coworkers [2] except that our experimental spectra show better resolution.

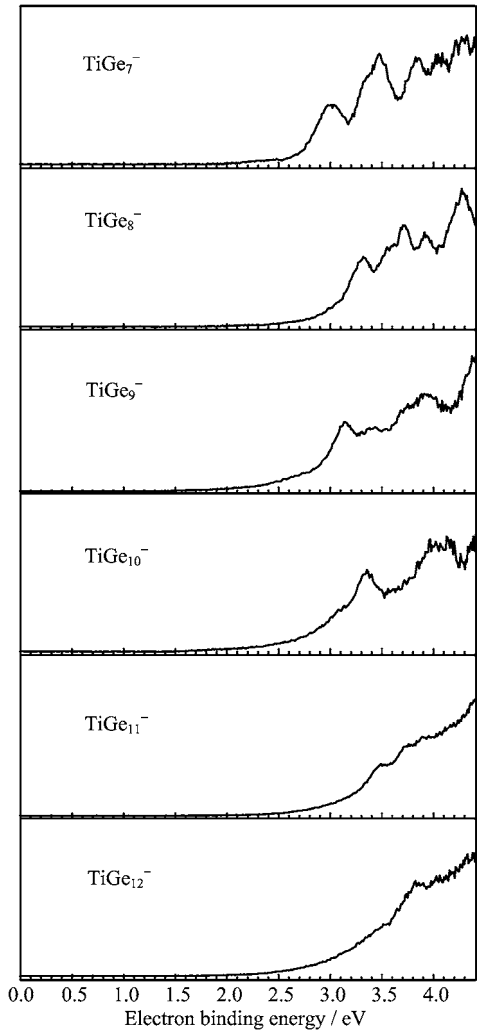

FIG. 1 Photoelectron spectra of $TiGe_n^-$ (n=7−12) clusters recorded with 266 nm photons.

TABLE I Experimentally observed VDEs and ADEs from the photoelectron spectra of $TiGe_n^-$ (n=7−12).

Cluster	VDE/eV	ADE/eV
$TiGe_7^-$	2.97±0.08	2.70±0.08
$TiGe_8^-$	3.32±0.08	3.00±0.08
$TiGe_9^-$	3.15±0.08	2.75±0.08
$TiGe_{10}^-$	3.12±0.08	2.67±0.08
$TiGe_{11}^-$	3.5±0.2	3.05±0.2
$TiGe_{12}^-$	3.5±0.2	3.30±0.2

As shown in Fig.1, there are four resolved peaks centered at 2.97, 3.47, 3.84, and 4.04 eV, and an unresolved peak over 4.27 eV in the spectrum of $TiGe_7^-$. With respect to the spectrum of $TiGe_8^-$, four peaks centered at

DOI:10.1063/1674-0068/29/cjcp1511232

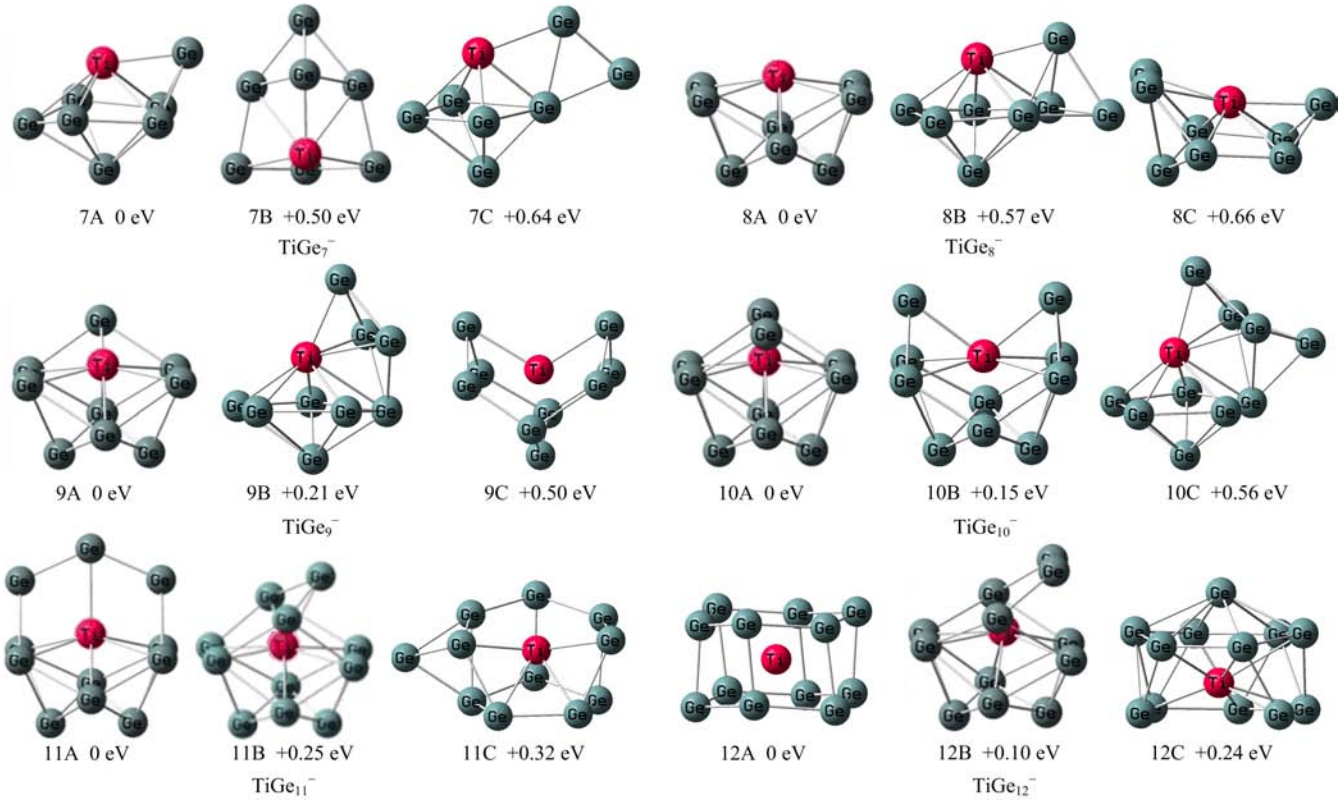

FIG. 2 Low-lying isomers of TiGe$_n^-$ (n=7−12) clusters. The relative energies to the most stable isomers are shown.

3.32, 3.70, 3.91, and 4.27 eV and a shoulder at 3.53 eV can be observed. As for TiGe$_9^-$, it has two major peaks centered at 3.15 and 3.91 eV, as well as two barely noticeable peaks at 3.40 and 4.37 eV. TiGe$_{10}^-$ has a major peak centered at 3.35 eV, a shoulder at 3.12 eV, a broad peak at 3.96 eV, and the onset of a high EBE peak above 4.3 eV. The spectral features of TiGe$_{11}^-$ are very broad with three barely discernible peaks centered at 3.5, 3.7, and 3.9 eV respectively. The spectral features of TiGe$_{12}^-$ are also very broad. It has a major peak centered at ∼3.8 eV and a shoulder at ∼3.5 eV.

B. Theoretical results

The typical low-lying isomers for the TiGe$_n^-$ (n=7−12) clusters obtained from the DFT calculations are presented in Fig.2 with the most stable ones on the left. Their theoretical VDEs and ADEs are summarized in Table II. The VDE is defined as the energy difference between the neutral and anion both at the equilibrium structure of the anion, whereas the ADE is the energy difference between the neutral and the anion with the neutral relaxed to the nearest local minimum using the anionic structure as initial structure. The Cartesian coordinates of the low-lying isomers are available in the supplementary material.

With respect to TiGe$_7^-$, isomer 7A can be regarded as a Ge atom capping the TiGe$_6$ pentagonal bipyramid with the Ti atom at the vertex, and its calculated VDE (2.70 eV) is in reasonable agreement with the experimental value (2.97 eV). Isomers 7B and 7C are much less stable than 7A by 0.50 and 0.64 eV in energy, respectively. Thus, we suggest that 7A is the dominant structure observed in our experiments.

The most stable isomer (8A) of TiGe$_8^-$ can be viewed as a half-endohedral structure with the Ti atom locating in a boat-shaped Ge$_8$ framework, and its theoretical VDEs of 8A (3.15 eV) is in agreement with the experimental value (3.32 eV). Isomer 8B can be seen as two Ge atoms capping on a TiGe$_6$ pentagonal bipyramid. The energies of 8B and 8C are much higher than that of 8A by 0.57 and 0.66 eV, respectively. Therefore, we suggest that 8A is the major structure contributed to the experimental spectrum.

For TiGe$_9^-$, the most stable isomer 9A can be viewed as a Ge atom capping the boat-shaped structure of TiGe$_8^-$ (8A). Isomer 9B can be obtained by connecting a Ge$_3$ triangular to a TiGe$_6$ pentagonal bipyramid, and its energy is higher than 9A by 0.21 eV. Isomer 9C is less stable than isomer 9A by 0.50 eV, thus the existence of 9C can be ruled out. The theoretical VDEs of isomers 9A and 9B are 2.97 and 3.31 eV, respectively, both close to the experimental value (3.15 eV). Therefore, isomer 9A is suggested to be the most probable one detected in our experiments, but the existence of

DOI:10.1063/1674-0068/29/cjcp1511232

TABLE II Relative energies, VDEs and ADEs of the low energy isomers of the $TiGe_n^-$ (n=7−12) obtained by DFT calculations. Multiplicities are 2.

Isomer		Sym.	ΔE/eV	VDE/eV		ADE/eV	
				Theo.	Expt.	Theo.	Expt.
$TiGe_7^-$	7A	C_s	0.00	2.70	2.97	2.54	2.70
	7B	C_s	0.50	2.63		2.46	
	7C	C_s	0.64	2.83		2.63	
$TiGe_8^-$	8A	C_{2v}	0.00	3.15	3.32	3.02	3.00
	8B	C_s	0.57	2.76		2.64	
	8C	C_s	0.66	3.22		2.93	
$TiGe_9^-$	9A	C_s	0.00	2.97	3.15	2.92	2.75
	9B	C_s	0.21	3.31		2.96	
	9C	C_{2v}	0.50	3.25		3.17	
$TiGe_{10}^-$	10A	C_{2v}	0.00	3.20	3.12	3.13	2.67
	10B	C_{2v}	0.15	3.38		3.25	
	10C	C_1	0.56	2.87		2.80	
$TiGe_{11}^-$	11A	C_s	0.00	3.80	3.5	3.34	3.05
	11B	C_1	0.25	3.04		2.67	
	11C	C_1	0.32	3.33		3.17	
$TiGe_{12}^-$	12A	C_{2h}	0.00	3.43	3.5	3.25	3.30
	12B	C_s	0.10	3.40		3.07	
	12C	C_s	0.24	3.40		2.93	

isomer 9B cannot be ruled out.

As for $TiGe_{10}^-$, the structures of isomers 10A and 10B can be described as two Ge atoms connecting to the different locations of the boat-shaped structure of $TiGe_8^-$ (8A), and isomer 10B is higher than isomer 10A in energy by only 0.15 eV. The calculated VDE of isomer 10A (3.20 eV) is in good agreement with the experimental value (3.12 eV). That of isomer 10B is calculated to be 3.38 eV. Isomer 10C is much less stable than 10A by 0.56 eV in energy. Thus, we suggest that isomer 10A is the major species in our experiments and isomer 10B may contribute to the higher EBE peaks in the experimental spectrum.

For $TiGe_{11}^-$, both isomers 11A and 11B can be regarded as three Ge atoms connecting to the top of the boat-shaped structure of $TiGe_8^-$ (8A). The calculated VDE of 11A (3.80 eV) is in reasonable agreement with the experimental value (3.5 eV). Isomer 11B is higher in energy than isomer 11A by 0.25 eV and its theoretical VDE (3.04 eV) is much lower than the experimental value. Isomer 11C is less stable than 11A by 0.32 eV. Therefore, isomer 11A is the most likely structure of $TiGe_{11}^-$ in our experiments.

The most stable structure of $TiGe_{12}^-$ (12A) is a distorted hexagonal prism structure with the Ti atom at the center. Isomer 12B can be seen as four Ge atoms connecting to the top of boat-shaped structure of $TiGe_8^-$ (8A). The calculated VDEs of 12A (3.43 eV), 12B (3.40 eV) and 12C (3.40 eV) are all consistent with the experimental value (3.5 eV). Isomer 12B is higher than that isomer 12A by only 0.10 eV while isomer 12C is higher than 12A by 0.24 eV. Therefore, we suggest that 12A is the dominant structure observed in our experiments, but the existence of 12B cannot be ruled out.

We have also investigated the structures of neutral $TiGe_n$ (n=7−12) clusters and displayed them in Fig.3. It can be seen that the most stable structures of the neutral $TiGe_n$ (n=7−12) clusters are similar to those of the $TiGe_n^-$ anions, except that those of $TiGe_{11}$ and $TiGe_{12}$ are different from their anionic counterparts. The most stable structure of neutral $TiGe_{11}$ cluster (11A′) is similar to the second stable structure of $TiGe_{11}^-$ anion (11B). For neutral $TiGe_{12}$, the most stable structure (12A′) is similar to the second stable structure of $TiGe_{12}^-$ anion (12B), while the second stable structure (12B′) is similar to the most stable one of $TiGe_{12}^-$ anion (12A). Isomer 12B′ is higher in energy than 12A′ by only 0.08 eV. The most stable structures of the neutral $TiGe_n$ (n=7−12) clusters found in this work are slightly different from those reported in Ref.[12]. In Ref.[12], the ground state structure of $TiGe_8$ can be seen as a Ge atom capping a $TiGe_7$ hexagonal bipyramid, which is different from the half-encapsulated boat-shaped structure in this work. We found that the most stable structures of $TiGe_n$ (n=9−12) clusters are all derived from the boat-shaped structure of $TiGe_8$. In Ref.[12], the ground structures of $TiGe_9$ and $TiGe_{10}$ can also be seen as deriving from the boat-shaped structure of $TiGe_8$, but they are slightly distorted compared with the most stable structures in this work. While the ground structure of $TiGe_{11}$ in Ref.[12] can be described as a basket-shaped structure. Also, the ground state structure of neutral $TiGe_{12}$ reported previously is a distorted hexagonal prism, which is similar to the most stable structure of anionic $TiGe_{12}^-$ (12A) and the second stable structure of neutral $TiGe_{12}$ (12B′) in this work. Such different results are probably because we used a larger basis set in this work.

IV. DISCUSSION

As shown in Fig.3, the Ti atom is half-encapsulated by a boat-shaped Ge_8 framework at n=8, and the opening of the boat-shaped structure is gradually covered by the additional Ge atoms to form Ge_n cage from n=9 to 11. At n=8−12, the endohedral structures of both anionic and neutral $TiGe_n$ clusters are more stable than their exohedral structures. For anionic and neutral $TiGe_{12}$ cluster, the Ti atom is completely encapsulated by the Ge_{12} cage, in which the anionic $TiGe_{12}$ has a distorted hexagonal prism cage structure while the neutral $TiGe_{12}$ has a Ge_4 capped boat-shaped structure. The structural evolution found in this work agrees with the adsorption reactivity of neutral $TiGe_n$ (n=7−16) towards H_2O [2], in which the reactivity generally decreases with an increasing number of Ge atoms from

DOI:10.1063/1674-0068/29/cjcp1511232

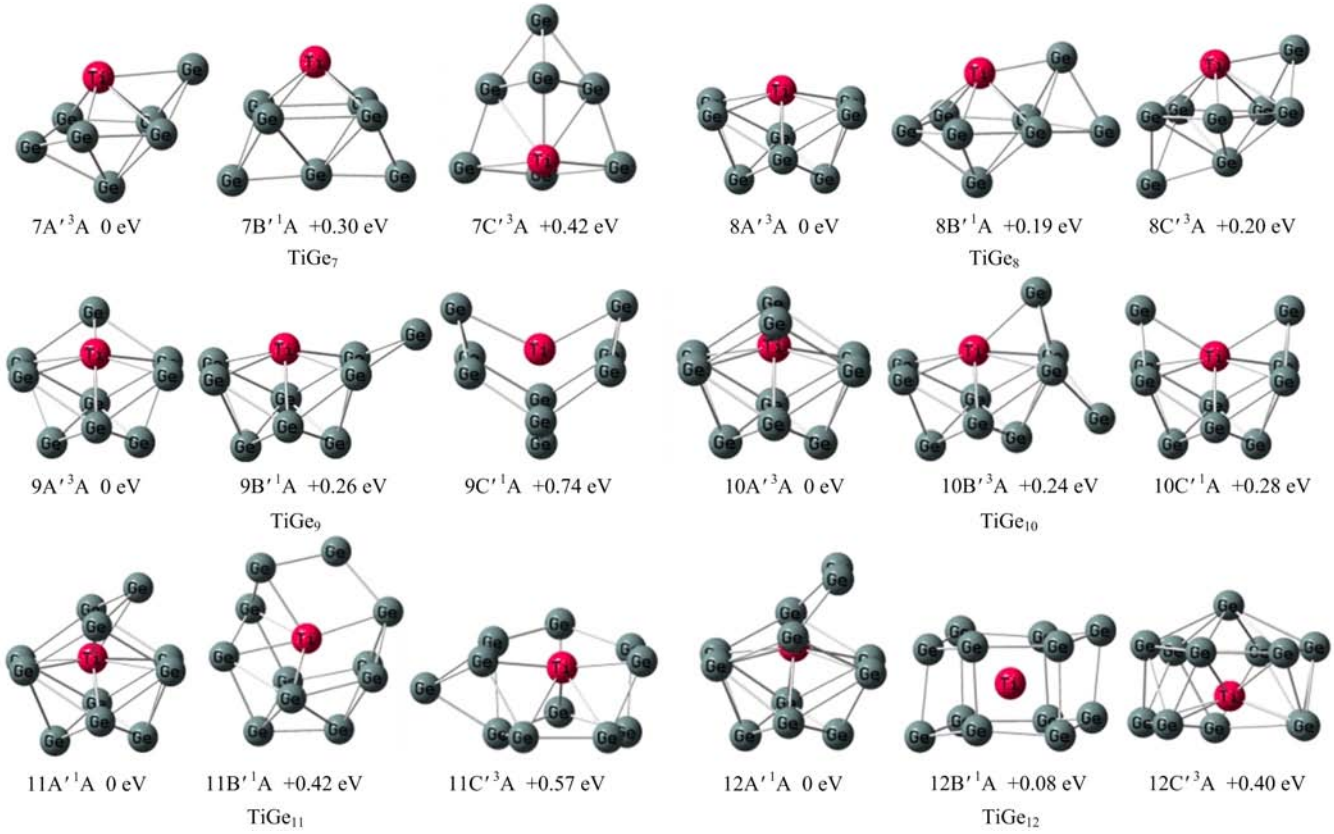

FIG. 3 Low-lying isomers of neutral TiGe$_n$ (n=7−12) clusters. The relative energies to the most stable isomers are shown.

n=7−11, and the relative reactivity is lost at n=12.

We also investigated the electronic and magnetic properties of the most stable structures of anionic and neutral TiGe$_n$ (n=7−12) clusters using NPA. As shown in Table III, for both anionic and neutral TiGe$_n$ clusters size with n=8−12, the negative charge on Ti atom increases significantly, suggesting that there is more electron transfer from the Ge atoms to the Ti atom. This also indicates that the electron transfer from the Ge$_n$ framework to the Ti atom is strongly related to the structural evolution of TiGe$_n$ clusters, especially related to the formation of endohedral structures. In addition, this electron transfer pattern is similar to those of CoGe$_n^{-/0}$ (n=2−11) [26] and VGe$_n^{-/0}$ (n=3−12) [27] clusters, but different from those of the CuGe$_n$ (n=2−13) [20], and NiGe$_n$ (n=1−20) [32] clusters, in which the electron transfers from the Cu or Ni atom to the Ge$_n$ framework. As shown in Table III, the total magnetic moments of the anion TiGe$_n^-$ (n=7−12) clusters are 1 μ_B. As for the neutral TiGe$_n$ clusters, our calculations show that the multiplicities of the most stable isomers of TiGe$_7$ to TiGe$_{10}$ are 3, while those of TiGe$_{11}$ and TiGe$_{12}$ are 1; thus, the total magnetic moments are 2 μ_B for sizes of n=7−10, and 0 μ_B for n=11 and 12. The magnetic moment of TiGe$_{11}$ and TiGe$_{12}$ quench is possibly because there are more electrons transfer from the Ge atoms to the Ti atom and stronger connection between the Ge atoms and Ti atom. For both anionic and neutral TiGe$_n$ (n=7−12) clusters, the total magnetic moments are contributed by both Ti and Ge atoms.

TABLE III NPA charge of the Ti atom, atomic magnetic moments of the Ti atom (μ_{Ti}), total magnetic moments (μ_t) in the most stable isomers of the anionic and neutral TiGe$_n$ (n=7−12) clusters.

Cluster	NPA charge on Ti/e	μ_t/μ_B	μ_{Ti}/μ_B
TiGe$_7^-$	−0.84	1	0.77
TiGe$_8^-$	−1.23	1	0.92
TiGe$_9^-$	−2.18	1	0.47
TiGe$_{10}^-$	−3.42	1	0.62
TiGe$_{11}^-$	−2.89	1	0.67
TiGe$_{12}^-$	−3.14	1	0.42
TiGe$_7$	−0.39	2	1.68
TiGe$_8$	−1.21	2	0.93
TiGe$_9$	−2.11	2	1.05
TiGe$_{10}$	−3.20	2	1.14
TiGe$_{11}$	−4.88	0	0
TiGe$_{12}$	−3.82	0	0

DOI:10.1063/1674-0068/29/cjcp1511232

V. CONCLUSION

The structural, electronic and magnetic properties of anionic and neutral $TiGe_n$ (n=7−12) clusters were investigated using anion photoelectron spectroscopy in combination with density functional theory calculations. A half-endohedral boat-shaped structure emerged at n=8, then the opening of the boat-shaped structure is gradually capped by the additional Ge atoms to form Ge_n cage at n=9−11. $TiGe_{12}^-$ cluster has a distorted hexagonal prism cage structure. The electron transfer from the Ge_n cage to the Ti atom increases at n=8−12, suggesting that the electron transfer pattern is related to the structural evolution, especially to the formation of endohedral structure. For both anionic and neutral $TiGe_n$ (n=7−12) clusters, the total magnetic moments are contributed by both Ti and Ge atoms.

Supplementary materials: The Cartesian coordinates of the low-lying isomers are available.

VI. ACKNOWLEDGMENTS

Wei-jun Zheng acknowledges the Knowledge Innovation Program of the Chinese Academy of Sciences (No.KJCX2-EW-H01) and Hong-guang Xu acknowledges the National Natural Science Foundation of China (No.21103202) for financial support. The theoretical calculations were conducted on the ScGrid and DeepComp 7000 of the Supercomputing Center, Computer Network Information Center of the Chinese Academy of Sciences.

[1] X. Zhang, G. L. Li, and Z. Gao, Rapid Commun. Mass Spectrom. **15**, 1573 (2001).
[2] J. Atobe, K. Koyasu, S. Furuse, and A. Nakajima, Phys. Chem. Chem. Phys. **14**, 9403 (2012).
[3] J. Wang and J. G. Han, J. Phys. Chem. B **110**, 7820 (2006).
[4] W. J. Zhao and Y. X. Wang, Chem. Phys. **352**, 291 (2008).
[5] G. L. Li, X. Zhang, Z. C. Tang, and Z. Gao, Chem. Phys. Lett. **359**, 203 (2002).
[6] X. R. Li, Y. D. Ma, Y. Dai, and B. B. Huang, J. Mater. Chem. C **1**, 4565 (2013).
[7] W. J. Lin, B. L. Wang, K. J. Qiu, F. Y. Zhou, L. Li, J. P. Lin, Y. B. Wang, and Y. F. Zheng, J. Biomed. Mater. Res. Part B **100B**, 2239 (2012).
[8] C. L. Yan, W. Xi, W. P. Si, J. W. Deng, and O. G. Schmidt, Adv. Mater. **25**, 539 (2013).
[9] V. Kumar and Y. Kawazoe, Phys. Rev. Lett. **88**, 235504 (2002).
[10] D. Bandyopadhyay, P. Kaur, and P. Sen, J. Phys. Chem. A **114**, 12986 (2010).
[11] C. M. Tang, M. Y. Liu, W. H. Zhu, and K. M. Deng, Comput. Theor. Chem. **969**, 56 (2011).
[12] M. Kumar, N. Bhattacharyya, and D. Bandyopadhyay, J. Mol. Model. **18**, 405 (2012).
[13] S. Furuse, K. Koyasu, J. Atobe, and A. Nakajima, J. Chem. Phys. **129**, 064311 (2008).
[14] X. J. Deng, X. Y. Kong, X. L. Xu, H. G. Xu, and W. J. Zheng, RSC Adv. **4**, 25963 (2014).
[15] H. G. Xu, Z. G. Zhang, Y. Feng, J. Y. Yuan, Y. C. Zhao, and W. J. Zheng, Chem. Phys. Lett. **487**, 204 (2010).
[16] C. T. Lee, W. T. Yang, and R. G. Parr, Phys. Rev. B **37**, 785 (1988).
[17] A. J. H. Wachters, J. Chem. Phys. **52**, 1033 (1970).
[18] A. D. Becke, J. Chem. Phys. **98**, 5648 (1993).
[19] M. J. Frisch, G. W. Trucks, H. B. Schlegel, G. E. Scuseria, M. A. Robb, J. R. Cheeseman, J. A. Montgomery Jr., T. Vreven, K. N. Kudin, J. C. Burant, J. M. Millam, S. S. Iyengar, J. Tomasi, V. Barone, B. Mennucci, M. Cossi, G. Scalmani, N. Rega, G. A. Petersson, H. Nakatsuji, M. Hada, M. Ehara, K. Toyota, R. Fukuda, J. Hasegawa, M. Ishida, T. Nakajima, Y. Honda, O. Kitao, H. Nakai, M. Klene, X. Li, J. E. Knox, H. P. Hratchian, J. B. Cross, V. Bakken, C. Adamo, J. Jaramillo, R. Gomperts, R. E. Stratmann, O. Yazyev, A. J. Austin, R. Cammi, C. Pomelli, J. W. Ochterski, P. Y. Ayala, K. Morokuma, G. A. Voth, P. Salvador, J. J. Dannenberg, V. G. Zakrzewski, S. Dapprich, A. D. Daniels, M. C. Strain, Ö. Farkas, D. K. Malick, A. D. Rabuck, K. Raghavachari, J. B. Foresman, J. V. Ortiz, Q. Cui, A. G. Baboul, S. Clifford, J. Cioslowski, B. B. Stefanov, G. Liu, A. Liashenko, P. Piskorz, I. Komaromi, R. L. Martin, D. J. Fox, T. Keith, M. A. Al-Laham, C. Y. Peng, A. Nanayakkara, M. Challacombe, P. M. W. Gill, B. Johnson, W. Chen, M. W. Wong, C. Gonzalez, and J. A. Pople, *Gaussian* 03, Pittsburgh, PA: Gaussian, Inc., (2004).
[20] J. Wang and J. G. Han, J. Chem. Phys. **123**, 244303 (2005).
[21] J. Wang and J. G. Han, J. Phys. Chem. A **110**, 12670 (2006).
[22] Q. Jing, F. Y. Tian, and Y. X. Wang, J. Chem. Phys. **128**, 124319 (2008).
[23] W. J. Zhao and Y. X. Wang, J. Mol. Struct.: THEOCHEM **901**, 18 (2009).
[24] N. Kapila, V. K. Jindal, and H. Sharma, Physica B **406**, 4612 (2011).
[25] D. Bandyopadhyay, J. Mol. Model. **18**, 3887 (2012).
[26] X. J. Deng, X. Y. Kong, X. L. Xu, H. G. Xu, and W. J. Zheng, ChemPhysChem **15**, 3987 (2014).
[27] X. J. Deng, X. Y. Kong, H. G. Xu, X. L. Xu, G. Feng, and W. J. Zheng, J. Phys. Chem. C **119**, 11048 (2015).
[28] J. P. Foster and F. Weinhold, J. Am. Chem. Soc. **102**, 7211 (1980).
[29] A. E. Reed and F. Weinhold, J. Chem. Phys. **78**, 4066 (1983).
[30] A. E. Reed and F. Weinhold, J. Chem. Phys. **83**, 1736 (1985).
[31] A. E. Reed, R. B. Weinstock, and F. Weinhold, J. Chem. Phys. **83**, 735 (1985).
[32] A. E. Reed, L. A. Curtiss, and F. Weinhold, Chem. Rev. **88**, 899 (1988).
[33] F. Weinhold and J. E. Carpenter, *The Structure of Small Molecules and Ions*, R. Naaman and Z. Vager, Eds., 227 (1988).
[34] J. E. Carpenter and F. Weinhold, J. Mol. Struct. THEOCHEM **169**, 41 (1988).

DOI:10.1063/1674-0068/29/cjcp1511232